ACS APPLIED MATERIALS & INTERFACES

Research Article

www.acsami.org

Shish-Kebab-Structured Poly(ε-Caprolactone) Nanofibers Hierarchically Decorated with Chitosan−Poly(ε-Caprolactone) Copolymers for Bone Tissue Engineering

Xin Jing,[†,‡] Hao-Yang Mi,[†,‡] Xin-Chao Wang,[§] Xiang-Fang Peng,*[,†] and Lih-Sheng Turng*[,‡]

[†]National Engineering Research Center of Novel Equipment for Polymer Processing, The Key Laboratory for Polymer Processing Engineering of Ministry of Education, South China University of Technology, Guangzhou, 510640, China

[‡]Wisconsin Institute for Discovery, University of Wisconsin−Madison, Madison, Wisconsin 53715, United States

[§]National Engineering Research Center for Advanced Polymer Processing Technologies, Zhengzhou University, Zhengzhou, 450002, China

Supporting Information

ABSTRACT: In this work, scaffolds with a shish-kebab (SK) structure formed by poly(ε-caprolactone) (PCL) nanofibers and chitosan−PCL (CS−PCL) copolymers were prepared via electrospinning and subsequent crystallization for bone tissue engineering applications. The aim of this study was to introduce nanosized topography and the high biocompatibility of chitosan onto PCL nanofibers to enhance cell affinity to PCL scaffolds. CS−PCL copolymers with various ratios were synthesized, and then spontaneously crystallized as kebabs onto the electrospun PCL fibers, which acted as shishes. Scanning electron microscopy (SEM) results demonstrated that the copolymer with PCL to chitosan ratio of 8.8 could hierarchically decorate the PCL nanofibers and formed well−shaped kebabs on the PCL nanofiber surface. Water contact angle tests and biomimetic activity experiments revealed that the shish-kebab scaffolds with CS−PCL kebabs (PCL−SK(CS−$PCL_{8.8}$)) showed enhanced hydrophilicity and mineralization ability compared with smooth PCL and PCL−SK(PCL) shish-kebab scaffolds. Osteoblast-like MG63 cells cultured on the PCL−SK(CS−$PCL_{8.8}$) scaffolds showed optimizing cell attachment, cell viability, and metabolic activity, demonstrating that this kind of scaffold has potential applications in bone tissue engineering.

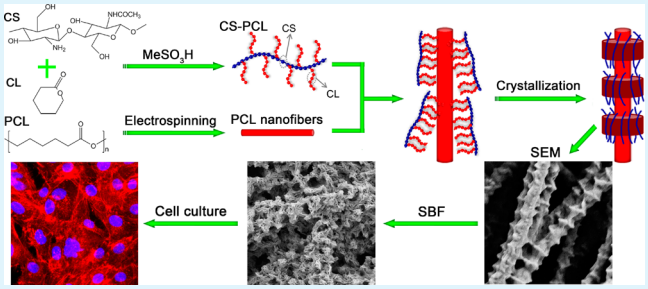

KEYWORDS: *poly(ε-caprolactone)(PCL), chitosan (CS), electrospinning, shish-kebab structure, tissue engineering*

1. INTRODUCTION

The optimum choice for bone repair is the employment of autogenous bone grafts. However, autogenous bone grafting has limitations, such as significant clinical morbidity, prolonged hospitalization, delayed rehabilitation, and surgical complications. Tissue engineering provides an alternative option for fabricating scaffolds for bone tissue replacement. The fabricated tissue engineering scaffolds should have the following characteristics: (1) appropriate levels and sizes of porosity allowing for cell migration and the transport of nutrients and metabolic waste, (2) a suitable surface area and surface chemistry that encourage cell adhesion, growth, migration, and differentiation, and (3) sufficient mechanical properties to support the surrounding native tissue.[1,2] Electrospinning is a commonly used technique for fabricating scaffolds for tissue engineering purposes.[3−6] The great advantage of electrospinning over other techniques is that the prepared structure features a morphology similar to extracellular matrix (ECM).[7]

Electrospun synthetic polymers, such as poly(ε-caprolactone) (PCL), poly(lactic acid) (PLA), and poly(D,L-lactide-*co*-glycolide) (PLGA), have been extensively investigated for use in tissue engineering due to their good mechanical properties and biocompatibility.[8] Despite being biocompatible and biodegradable, cell affinity toward these synthetic scaffolds are generally poor because of their low hydrophilicity and lacking of cell recognition sites.[9] Methods such as surface coating, blending, and chemical grafting have been used to modify these scaffolds. For the surface coating method, the scaffold is immersed in a solution containing biomolecules, such as collagen, gelatin, chitosan, or natural adhesive protein. This method is simple but the coated layer is not stable and easily detaches under physiological conditions.[10] To fabricate a hybrid scaffold containing both synthetic and natural polymers, the components need to be dissolved in their respective cosolvents, leading to a blended system that suffers from phase separation and nonuniform dispersion of biomolecules due to their differences in physiochemical properties (e.g., dissolvability, hydrophilicity).[11,12] To chemically graft the biomolecules on a

Received: January 31, 2015
Accepted: March 11, 2015
Published: March 11, 2015

DOI: 10.1021/acsami.5b00900
ACS Appl. Mater. Interfaces 2015, 7, 6955−6965

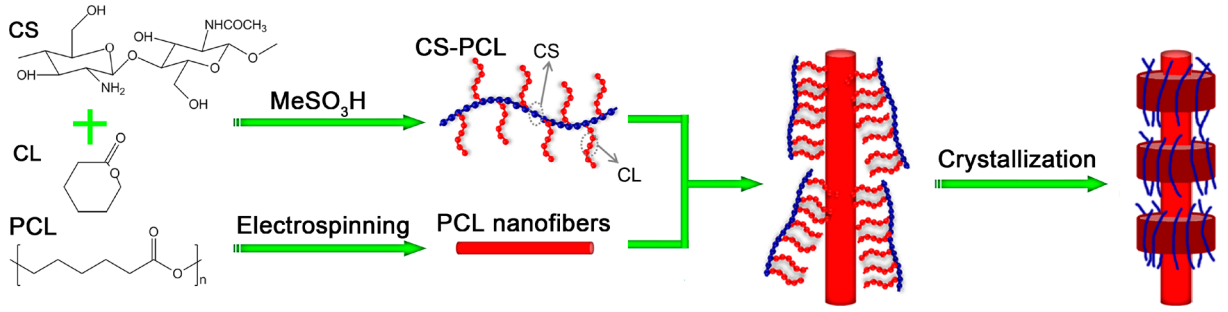

Figure 1. Schematic of preparing shish-kebab structured scaffolds using CS−PCL copolymers.

polyester scaffold, carboxylates and hydroxyl groups need to be introduced via hydrolysis and then the biomolecules can be bonded to these groups. However, during activation, the polymer backbone is affected which sacrifices the mechanical strength of the scaffolds.[13−15]

Surface topography is another important factor that influences the adhesion and subsequent behavior of cells. The nanoscale topography of the scaffold surface has been found to have significant positive effects on the response of osteoblast cell, including initial cell adhesion and subsequent proliferation, as well as expression of differentiation markers. The beneficial effect of the material surface nanotopography on cell colonization has been ascribed to an increased amount of protein adsorption, such as fibronectin and vitronectin, and an improved spatial conformation of the adsorbed cell adhesion-mediating proteins.[16,17] However, the surface of electrospun fibers is smooth, which is not beneficial for cell adhesion. Inspired by cell behavior on rugged surfaces and the morphology of the shish-kebab structure,[18,19] our group introduced the shish-kebab structure onto electrospun PCL scaffolds via controlled PCL crystallization. The resulting scaffolds were favorable for 3T3 mouse fibroblast cell and human fibroblast cell growth.[13,20] In the PCL shish-kebab structure, PCL electrospun nanofibers acted as shishes, while the kebabs had PCL lamellae crystals growing epitaxially on the PCL shishes.

To the best of our knowledge, few studies have been devoted to studying the use of the shish-kebab structure in electrospun scaffolds to enhance the surface roughness for bone tissue engineering applications. Although the kebabs on the surface enhanced cell adhesion on PCL scaffolds to some extent, the lack of integrin binding sites on the surface of the prepared scaffolds is still a major shortcoming for tissue engineering applications. Therefore, to combine the advantages of good biocompatibility of natural polymers (rich in cell recognition sites) and the enhanced surface roughness of the shish-kebab structure, we proposed to use a copolymer of natural and synthetic polymers to crystallize on the surface of the electrospun nanofibers. The prepared structure is expected to not only provide integrin binding sites for cell growth from the natural polymer but also to introduce the shish-kebab structure to facilitate cell adhesion.

PCL is a bioresorbable polymer with potential applications for bone and cartilage repair.[21,22] Compared with other synthetic biocompatible polymers, PCL has excellent mechanical properties and degrades at a rate compatible with bone regeneration.[23] Much research has been focused on the use of PCL biocomposites and copolymers of PCL with both natural and synthetic polymers[24,25] to enhance the cell response on PCL scaffolds. Chitosan is a deacetylated derivative of naturally occurring polysaccharide chitin. The polycationic character of chitosan in combination with the presence of reactive functional groups, including hydroxyl and amine groups, enhanced both adherence to negatively charged molecules and cell adhesion.[26] Many attempts have been made to introduce chitosan into PCL scaffolds to enhance cell growth. For example, mouse preosteoblast cells on PCL−chitosan hybrid electrospun fibers exhibited elevated cell activity compared to pure PCL scaffolds[26] and SaOs-2 osteosarcoma cells showed the highest alkaline phosphatase (ALP) activities on the PCL/chitosan/PCL layer by layer nanofibrous scaffolds.[27]

In this study, caprolactone and chitosan copolymers with various ratios were synthesized. Then the copolymers were used to periodically crystallize on the electrospun PCL nanofibers to yield the desired periodic shish-kebab structure. The properties and morphologies of the copolymers and scaffolds were characterized by ^{1}H nuclear magnetic resonance (^{1}H NMR), X-ray photoelectron spectroscopy (XPS), differential scanning calorimetry (DSC), polarized optical microscopy (POM), scanning electron microscopy (SEM), and water contact angle tests. The bone-binding ability of the scaffolds was investigated via incubating in simulated body fluid (SBF). Moreover, MG63, osteblast-like cells, were seeded on the scaffolds for up to 14 days to study cell behaviors including cell attachment, viability, proliferation, as well as cell morphology by cytoskeleton study and SEM. The metabolic activity of the cells cultured on the scaffolds was evaluated by measuring their alkaline phosphatase activity and osteocalcin expression to explore their potential application in bone tissue engineering.

2. MATERIALS AND METHODS

2.1. Materials. PCL (M_n = 80 000), chitosan (M_n = 50 000−190 000, low molecular weight) with a viscosity of 20−300 cP (1 wt % in 1% acetic acid), methanesulfonic acid ($MeSO_3H$, 99.5%), ε-caprolactone (ε-CL), chloroform (ACS regent), *N*,*N*-dimethylformamide (DMF) (ACS regent), and acetic acid (ACS regent) were purchased from Sigma-Aldrich (Milwaukee, WI, U.S.A.). Other chemicals involved in this study were also purchased from Sigma-Aldrich unless otherwise stated.

2.2. Preparation of CS−PCL Copolymers. CS−PCL was synthesized by grafting ε-caprolactone oligomers onto CS via ring-opening polymerization following the methods used in previous studies.[28,29] In a typical reaction procedure, vacuum-dried chitosan (600 mg, 3.5 mmol of glucosamine units, taking into account the % DD, degree of deacetylation 80% via analysis of their ^{1}H NMR spectra) and $MeSO_3H$ were put into a flame-dried 50 mL round-bottom flask equipped with a Teflon-coated magnetic stirring bar. The mixture was stirred at 45 °C for 30 min to allow the CS to be completely dissolved, followed by the addition of distilled ε-CL monomer (4.79 g, 42 mmol, 12 equiv). The reaction mixture was stirred at 45 °C under nitrogen atmosphere for 5 h. Then, the mixture

DOI: 10.1021/acsami.5b00900
ACS Appl. Mater. Interfaces 2015, 7, 6955−6965

was transferred into a solution containing 100 mL of 0.2 M KH_2PO_4, 16 mL of 10 M NaOH, and 100 g of crushed ice. The resulting CS−PCL (1:12) copolymer was collected by vacuum filter and washed with deionized water several times until the pH reached 7. The final products were dried using a freeze drier at −56 °C for 1 week. Graft copolymer CS−PCL (1:36) was also synthesized according to a similar procedure by using different molecular ratios of chitosan and ε-CL monomer.

2.3. Preparation of PCL Nanofibrous Scaffolds by Electrospinning. A PCL solution with a concentration of 12 wt % was prepared by dissolving PCL pellets into a mixture of chloroform and dimethylformamide (DMF) (v/v = 6/4) and stirring for 12 h at room temperature. The solution was loaded into a 6 mL syringe connected by Teflon tubing to an 18 gauge blunt needle. A flow rate of 0.5 mL/h was obtained using a digital syringe pump (Harvard Bioscience Company). The applied voltage was 18 kV. Grounded aluminum foil and round stainless steel washers (inner diameter of 8.33 mm, McMaster-Carr, U.S.A.), kept 17 cm away from the needle tip, were used as collectors.

2.4. Preparation of Scaffolds with Shish-Kebab Structure. The shish-kebab structured scaffolds were prepared by hieratically decorated PCL nanofibers with controlling pure PCL and CS−PCL copolymers crystallization on the surface. The preparation process is shown in Figure 1. Dilute PCL, CS−PCL (1:12), and CS−PCL (1:36) copolymer solutions were used to form different shish-kebab structures on the surface of the electrospun PCL nanofibers. Briefly, 0.5 wt % PCL and the copolymers were dissolved in aqueous acetic acid (acetic acid: deionized water =77:23 v/v) at 40 °C for 1 h, respectively. Then, the solutions were cooled down to room temperature and the PCL nanofibers were incubated in the prepared solutions for 2 min. After incubation, the scaffolds were taken out from the corresponding solutions and placed into a vacuum oven at room temperature for 24 h to evaporate the solvent. The shish-kebab structure was formed during the incubation and drying procedures. The prepared shish-kebab structure using different solutions were named as PCL−SK (PCL), PCL−SK (CS−PCL 1:12), and PCL−SK (CS−PCL 1:36) based on the composition of kebabs, respectively.

2.3. Characterization Methods. *2.3.1. ^{1}H NMR and Fourier Transform Infrared (FTIR) Spectroscopy.* ^{1}H NMR spectra of various samples were collected on a Bruker DPX 300 spectrometer at 25 °C using deuterated DMSO (DMSO-d_6) (TMS, 99.9+%, NMR grade, Aldrich) as the solvent with tetramethylsilane as an internal reference. The ^{1}H NMR spectrum of chitosan was collected using 1% CD_3COOD/D_2O as the solvent. FTIR spectra were recorded in transmittance mode using a Bruker Tensor 27 spectrometer in the range of 4000−400 cm^{-1} with a resolution of 4 cm^{-1}.

After preparing the copolymer, its molecular weight (obtained from gel permeation chromatography, GPC) and average number of ε-CL units (CL_n) grafted onto one glucosamine unit of CS were summarized in Table 1. CL_n was determined by proto nuclear magnetic resonance (^{1}H NMR) using the following equation:[29]

$$CL_n = A_{[(a)/2]}/A_{[(3,4,5,6,6')/5]}$$

where $A_{[(a)/2]}$ represents half of integral area of protons in PCL units at 2.2 ppm and $A_{[(3,4,5,6,6')/5]}$ means one-fifth of the total integral area of protons 3, 4, 5, 6, and 6′ of saccharine units in CS at 3.4−3.9 ppm.

2.3.2. Gel Permeation Chromatography (GPC). GPC data were collected with a model VE2001 gel permeation chromatographer (GPC) equipped with a 302 tetra detector array. Tetrahydrofunan (THF, HPLC grade, Fisher Scientific) was used as an eluent and the flow rate was set at 1 mL/min with an injection volume of 100 μL. Calibrations of columns were carried out using a standard polystyrene (PS) solution. All test solutions were prepared at a concentration of 2.5 mg/mL.

To verify the stability of PCL and its copolymers in the cosolvent, GPC tests were performed to investigate the molecular weight change of PCL and its copolymers after dissolution into the cosolvent. The procedures were carried out as follows. First, pure PCL and its copolymers at a concentration of 0.5 wt % were dissolved into aqueous acetic acid (77% acetic acid) at 40 °C for 1 h. Then, the solutions were put into a vacuum oven at room temperature to evaporate the cosolvent completely. Next, the resulting pure PCL and CS−PCL copolymer powders were redissolved into THF to measure their molecular weight.

2.3.3. Morphological Characterization. The morphologies of the nanofibrous scaffolds were observed using a scanning electron microscope (SEM) after sputter coating with gold for 40 s. The scaffolds were observed on a fully digital LEO GEMINI (Zeiss, Germany) at a voltage of 3 kV. The fiber diameter was measured from the SEM images using Image-Pro Plus software. Fifty fibers were measured from three SEM images to obtain the fiber diameter distribution and average fiber diameter.

2.3.4. Differential Scanning Calorimetry (DSC) Tests. Differential scanning calorimetry (DSC) measurements were performed with a DSC Q20 (TA Instruments). Pure PCL and CS−PCL copolymers were heated to 150 °C at a heating rate of 5 °C/min and held isothermally for 3 min to eliminate any thermal history. Samples were then cooled down to −100 °C at 5 °C/min and reheated to 150 °C at the same rate. All tests were carried out under the protection of a nitrogen atmosphere.

2.3.5. X-ray Photoelectron Spectroscopy (XPS). The chemical compositions of the scaffolds were analyzed by X-ray photoelectron spectroscopy (XPS). XPS measurements were performed on an X-ray photoelectron spectrometer with a focused, monochromatic Kα X-ray source and a monatomic/cluster ion gun (Thermo Scientific, USA). Overlapping C peaks were resolved into their individual components by XPSPEAK 4.1 software.

2.3.6. Surface Wettability. Surface water contact angles (WCAs) of the nanofibrous scaffolds were assessed using the sessile drop method at room temperature with a video contact angle instrument (Dataphysics OCA 15). The droplet size was set at 4 μL. The surface contact angle was measured 15 s after dropping the deionized water. Three samples for each group were tested, and the average value was reported with standard deviation (SD).

2.3.7. Biomineralization Behavior Characterization. Biomineralization behavior was studied by incubating the scaffolds in the simulated body fluid (SBF) for up to 1 week. The procedure for SBF preparation was according to published ref 30. After incubating in 2 × SBF for 1 day, 3 days and 7 days, scaffolds were taken out and washed with deionized water twice. After drying, the scaffolds were sputter coated with gold and imaged with the aforementioned SEM. Energy dispersive X-ray spectroscopy (EDS) was performed to detect the compositions of the deposits on the scaffolds.

2.4. Biocompatibility Evaluations. With MG63 cells used as the cell model, cell morphology, cell viability, and proliferation, alkaline phosphatase (ALP) activity and osteocalcin expression were detected to investigate the biological performance of the pure PCL, PCL−SK(PCL), and PCL−SK (CS−PCL 1:36) scaffolds. The detailed experimental procedures of this section were shown in the Supporting Information.

Table 1. Characterization of Polycaprolactone Grafted Chitosan by GPC and ^{1}H NMR

	GPC analysis			
	M_n	M_w	PI	CL_n[a]
PCL	169766	254170	1.5	
CS−PCL (1:12)	7800	19420	2.5	6.5
CS−PCL (1:36)	8586	22313	2.6	8.8
PCL[b]	160808	241412	1.5	
CS-PCL[b] (1:12)	7024	18970	2.7	
CS-PCL[b] (1:36)[2]	7953	21473	2.7	

[a]Average number of CL units per glucosamine unit in CS, $CL_n = A_{[(a)/2]}/A_{[(3,4,5,6,6')/5]}$, calculated from ^{1}H NMR. [b]PCL means that the pure PCL was treated by aqueous acetic acid before running GPC tests.

DOI: 10.1021/acsami.5b00900
ACS Appl. Mater. Interfaces 2015, 7, 6955−6965

2.5. Statistical Analysis. All data obtained from the biological experiments in the study are shown as mean ± standard deviation (SD) unless specifically indicated otherwise. Statistical analyses were performed on the data using a one-way ANOVA. The difference between factors was analyzed by a Tukey test. A p-value of less than 0.05 and 0.01 was considered statistically significant.

3. RESULTS AND DISCUSSION

3.1. Chitosan Grafting with ε-Caprolactone (CS−PCL). Hydrophobic ε-CL was grafted onto the hydroxyl groups of CS via ring-opening reactions using methanesulfonic acid as both solvent and catalyst. Because of the protection of strong acidic media on the amino groups onto CS, the grafting reaction of ε-CL predominantly occurred on the hydroxyl groups of CS. The chemical structure of CS−PCL is shown in Figure 2. The

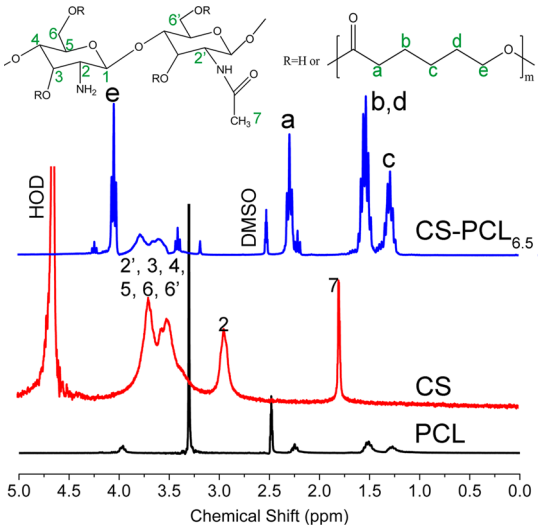

Figure 2. ^{1}H NMR spectra of PCL, CS, and CS−PCL$_{6.5}$ copolymers.

chemical shifts of ^{1}H NMR at 3.4−3.9 and 3.2 ppm were assigned to $H_{3,4,5,6,6'}$ and $H_{2'}$ of pyranose repeat units in CS, respectively.[31] The characteristic peaks of the PCL chains can be seen at 2.2 (H_a), 1.5 ($H_{b,d}$), 1.4 (H_c), and 4.0 (H_e).[32] The characteristic peaks of CS and PCL can be seen in the ^{1}HNMR curves of CS−PCL copolymers, indicating that PCL was covalently grafted onto CS. However, compared with pure chitosan, protons of chitosan in the copolymers experienced upfield shifts, which demonstrated the existence of a chemical reaction.

The molecular weight results of the neat PCL and CS−PCL copolymers with different CS to PCL feed ratios (1:12 and 1:36) are summarized in Table 1. Compared with CS−PCL (1:12), the CS−PCL (1:36) showed higher CL repeat unit numbers (CL_n) and increased molecular weights including M_n and M_w. To express the difference in molecular structure of CS−PCL copolymers, the CS−PCL (1:12) was renamed as CS−PCL$_{6.5}$ based on the ^{1}H NMR results (shown in Table 1), which means that one CS backbone contained 6.5 poly-caprolactone repeating units, and the CS−PCL (1:36) was renamed as CS−PCL$_{8.8}$. In Table 1, it was also found that after aqueous acetic acid treatment, the molecular weights of pure PCL and CS−PCL copolymers decreased slightly. However, on the basis of published report,[33] this slight degradation would not affect their biocompatibility.

FTIR was used to characterize the chemical structure of the CS−PCL copolymers, while CS and PCL were used as controls. The results are shown in Figure 3. The characteristic bands of the saccharine structure of CS appeared at 1154 and

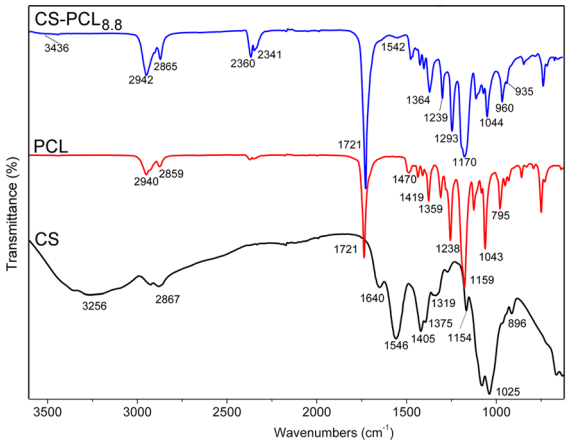

Figure 3. FTIR spectra of CS, PCL, and CS−PCL$_{8.8}$.

896 cm^{-1}, while the amide I band (C═O) and amino groups can be seen at 1640 and 1546 cm^{-1}, respectively.[34] The ester stretching at 1721 cm^{-1} on the PCL curve was regarded as a characteristic peak of PCL.[35] The FTIR spectra of CS−PCL copolymers exhibited obvious peaks at 1721, 1660, and 1542 cm^{-1}, which were assigned to the characteristic bands of ester in PCL, amide I band, and amino groups in CS, respectively. The intensity of stretching vibrations of C−O on 1721 cm^{-1} of CS−PCL copolymer became much stronger than that of PCL. These indicated the success of graft copolymerization of ε-CL monomer onto CS.

3.2. Crystallization Behavior of Pure PCL and CS−PCL Copolymers. The crystallization behavior of pure PCL and CS−PCL copolymers was investigated via DSC and the results are shown in Table 2. The degree of crystallinity of pure PCL

Table 2. Statistical Results of DSC Tests of Pure PCL and CS−PCL Copolymers

	T_c (°C)	T_m (°C)	$\chi_c{}^a$ (%)
PCL	27.3 ± 0.1*^{b}	57.3 ± 0.3*^{b}	41.4 ± 0.6*^{b}
CS−PCL$_{6.5}$	15.6 ± 0.4	38.5 ± 0.1	28.2 ± 0.8
CS−PCL$_{8.8}$	18.4 ± 0.2	42.7 ± 0.2	34.3 ± 0.3

$^a\chi_c = \Delta H_m/\Delta H_m^\circ$, where ΔH_m° = 139.5 J/g (heat of fusion for 100% crystalline PCL). ^{b}The Turkey test was run to compare the differences between PCL and CS−PCL copolymers. Values marked with an asterisk (*) were significantly different from the values of other groups ($p < 0.05$). Three samples from each group were tested to obtain the average value.

was significantly higher than that of CS−PCL copolymers. Meanwhile, for CS−PCL copolymers, their crystallinity degree increased with an increase of caprolactone content in the copolymers, indicating the hindrance of chitosan on the crystallization of PCL. The reason for this suppression might be the intermolecular hydrogen bonds between the carbonyl bonds of PCL and the hydroxyl groups on the chitosan chains, which affected the molecular mobility of PCL chains during crystallization. Another possible factor affecting PCL crystallization was that the relaxation temperature of the chitosan chains was much higher than the crystallization temperature of PCL. Hence, the amorphous regions of chitosan were in the glassy state at the crystallization temperature of PCL, resulting

DOI: 10.1021/acsami.5b00900
ACS Appl. Mater. Interfaces 2015, 7, 6955−6965

in the entrapment of PCL molecules, which further decreased the degree of crystallinity of the CS−PCL copolymers. The crystalline morphologies of PCL and CS−PCL copolymers are shown in Figure S1, which also demonstrated the differences of crystallization behavior of pure PCL and CS−PCL copolymers. Similar behaviors have also been observed in PCL and chitosan blends and other polyester−polysaccharide systems.[36−38]

3.3. Morphology of Nanofibrous Scaffolds. In this study, the synthesized CS−PCL copolymers were used to create a laminated kebab structure on electrospun PCL nanofibers by inducing crystallization as illustrated in Figure 1. The PCL chains on the CS backbone gradually attached and crystallized onto the PCL nanofibers as the solvent evaporated, which exposed the CS molecular chains outside of the kebabs, thus forming chitosan wrapped layers outside of the kebab surface. The morphologies of the shish-kebab structured scaffolds formed by different CS−PCL copolymers were compared with the smooth PCL nanofibers and the PCL nanofibers decorated by pure PCL solution. The results are shown in Figure 4.

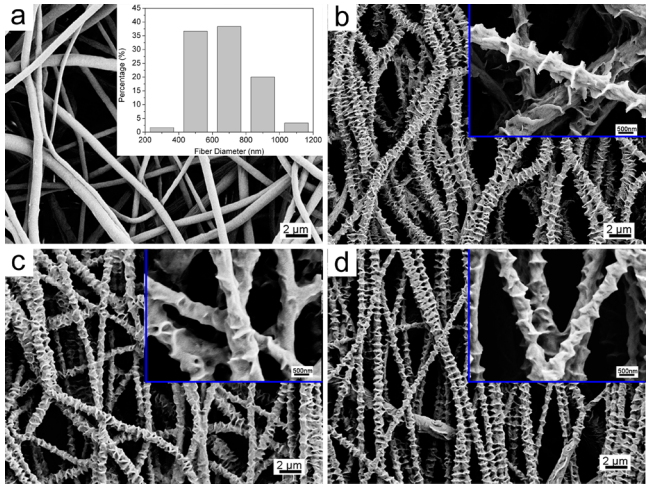

Figure 4. SEM micrographs of (a) PCL (the inset is the fiber diameter distribution of PCL scaffolds), (b) PCL−SK(PCL), (c) PCL−SK(CS−$PCL_{6.5}$), and (d) PCL−SK(CS−$PCL_{8.8}$). Scale bars in the inset images are 500 nm.

The original electrospun PCL nanofibers (Figure 4a) were smooth and beadless with the fiber diameter ranging from 200 nm to over 1000 nm. After incubating the electrospun PCL nanofibers in the diluted PCL, CS−$PCL_{6.5}$, and CS−$PCL_{8.8}$ solutions, the PCL and CS−PCL molecules crystallized on the surface of the nanofibers leading to the formation of hierarchically laminated kebabs. It was found that all three solutions could induce the formation of a shish-kebab structure as presented in Figure 4 b−d, respectively. The typical shish-kebab structure with CS−$PCL_{8.8}$ crystal lamellae grew perpendicularly to the PCL nanofiber axis was observed in Figure 4d, indicating CS−$PCL_{8.8}$ could attach and crystallize on PCL nanofibers easily. However, it is observed in Figure 4c that the CS−$PCL_{6.5}$ could not form regular kebabs on PCL nanofibers, which showed film-like flat kebabs. These differences might be caused by the difference in the crystallinity ability of the three kinds of polymers. For the CS−$PCL_{6.5}$ copolymer, the larger amount of chitosan resulted in the formation of chitosan film on the surface of PCL nanofibers.

The periodic distance and kebab size were measured to quantitatively investigate these differences. The measurements performed are illustrated in Figure 5a, and the related results

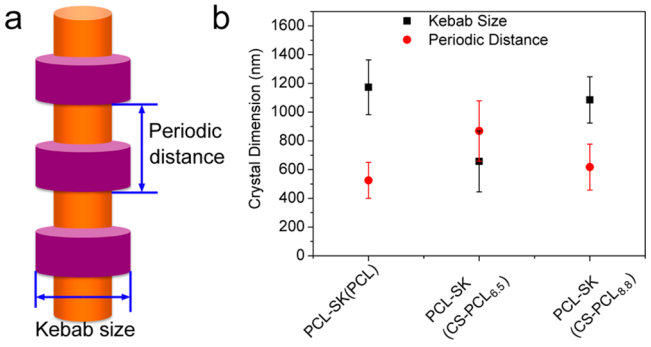

Figure 5. (a) Schematic of shish-kebab structure and (b) the kebab size and periodic distance of kebabs of the different compositions of the shish-kebab structured scaffolds.

are shown in Figure 5b. It was found that the kebab size of copolymer groups was smaller than those formed by PCL, especially for those formed by CS−$PCL_{6.5}$. Furthermore, the periodic distance of adjacent kebabs formed by copolymers was larger than those formed by neat PCL. In comparison, the kebabs formed by CS−$PCL_{6.5}$ were smaller and showed larger periodic distances than those formed by CS−$PCL_{8.8}$.

The reasons for the different shish-kebab structures prepared by the different kebab materials are as follows. During the formation of the shish-kebab structure, the compatibility of the shish and kebab materials is important because the kebab materials need to be adsorbed onto the shish surface prior to the crystallization process to nucleate on the nanofiber surface. The electrospun PCL nanofibers acted as shish in the process. The molecules in the kebab inducing solution precipitated from the dilute solution and attached to the PCL nanofiber surface because of physical interactions. Then the attached molecule chains were exclusively parallel to the long PCL nanofiber axes due to the geometric confinement of the nanofibers. As a result, a shish-kebab structure with crystal lamellae perpendicular to the long PCL nanofibers was obtained.[39] The mechanism for the formation of the shish-kebab structure has been elaborated upon in ref 39. However, the attachment behavior of PCL and CS−PCL onto the shish was different. For the CS−PCL copolymers, the PCL segments in the copolymers need to overcome the hindrance of the chitosan backbone to attach onto the PCL shish surface, which takes a much longer time than pure PCL. On the other hand, the crystallization ability of the copolymers is not as good as neat PCL (as indicated in Section 3.2) because of the negative effect of chitosan on the crystallization of PCL segments in the copolymers. In light of the geometrical and topographical similarity of PCL−SK (PCL) and PCL−SK (CS−$PCL_{8.8}$), the latter were used in the following experiments to compare with PCL−SK (PCL) scaffolds that exhibit a similar structure but with no chitosan.

3.4. Chemical Compositions of Scaffolds. The chemical compositions of the PCL, CS, and PCL−SK (CS−$PCL_{8.8}$) were characterized by XPS. Figure 6a shows the C 1s XPS spectra of the tested scaffolds. Besides the C−C, C−O, and C═O bonds endowed by the original PCL scaffolds, the scaffolds decorated with CS−PCL copolymer showed C−N bonds that belonged to the CS. This result confirmed the existence of CS on the surface of PCL−SK (CS−$PCL_{8.8}$) scaffolds. However,

DOI: 10.1021/acsami.5b00900
ACS Appl. Mater. Interfaces 2015, 7, 6955−6965

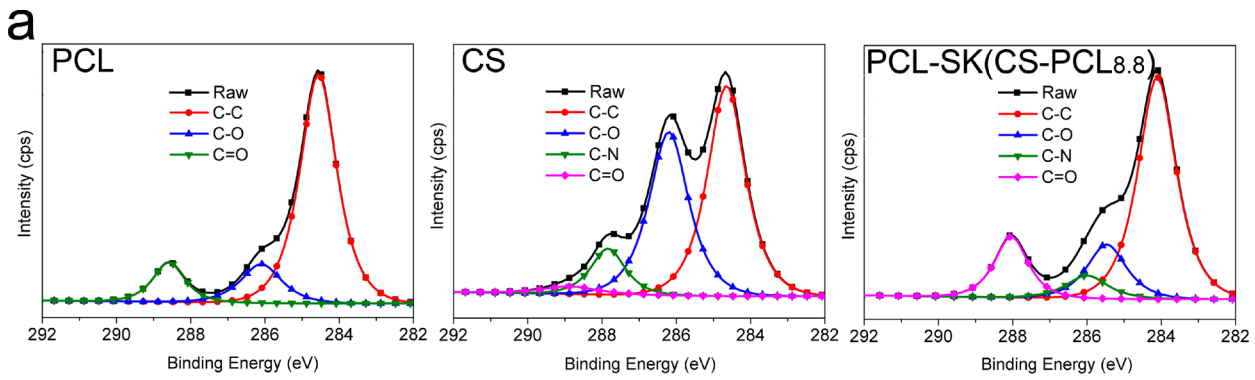

b

PCL

Bonds	Position	Area	Percentage
C–C	284.5	134027	74.9%
C–O	286.1	25054	14.0%
C=O	288.6	19920	11.1%

CS

Bonds	Position	Area	Percentage
C–C	284.6	82845	48.6%
C–O	286.2	67091	39.3%
C-N	287.8	16331	9.6%
C=O	288.8	4325	2.5%

PCL-SK(CS-PCL$_{8.8}$)

Bonds	Position	Area	Percentage
C–C	284.2	100000	62.3%
C–O	285.5	25884	16.1%
C–N	285.9	11172	7.0%
C=O	288.2	23334	14.6%

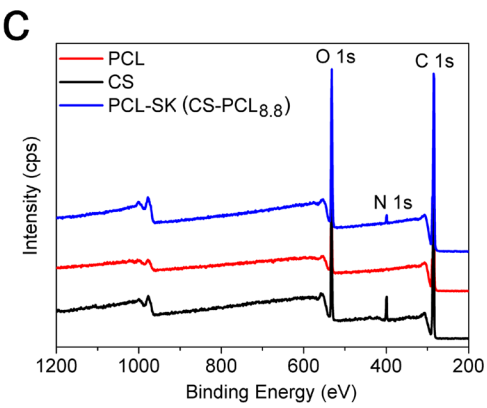

Figure 6. (a) High-resolution C 1s core level signals of PCL, CS, and PCL–SK (CS–PCL$_{8.8}$) scaffolds obtained from X-ray photoelectron spectra. (b) Compositions of functional groups of PCL, CS, and PCL–SK (CS–PCL$_{8.8}$). (c) The whole survey scans of PCL, CS, and PCL–SK (CS–PCL$_{8.8}$).

compared with neat CS, the peak of the C–N bond in PCL–SK (CS–PCL$_{8.8}$) shifted from 287.8 to 285.9 eV (shown in Figure 6b), which might have been caused by the interaction between CS and PCL during the reaction process. The survey scans were also carried out as shown in Figure 6c, from which it was noticed that the PCL–SK (CS–PCL) scaffolds showed not only C 1s and O 1s components, but also a N 1s component which belonged to CS, indicating that the CS–PCL had been crystallized on the surface of the PCL nanofibers.

3.5. Surface Wettability. The surface hydrophobicity of the scaffolds is well-known as a key factor for governing cell response, which can be assessed by measuring the contact angle through water spread of a droplet on the surface. The lower the contact angle, the more hydrophilic the surface is. As shown in Figure 7, PCL was found to be hydrophobic with a water contact angle of 129°. The water contact angle of PCL–SK (PCL) was 137° because of the increased roughness on the surface of the PCL–SK scaffolds. However, the contact angle of PCL–SK (CS–PCL$_{8.8}$) decreased to 64°, which can be attributed to the high hydrophilicity of chitosan. Previous studies have reported that a hydrophilic surface would facilitate cell adhesion on the scaffolds. For example, mouse osteoblasts on a hydrophilic surface demonstrated accelerated metabolic activity,[40] and osteodifferentiation and fibroblasts were found to have maximum cell adhesion when contact angles were between 60° and 80°.[41] Therefore, the enhanced hydrophilicity of the scaffolds should be favorable for cell attachment. The

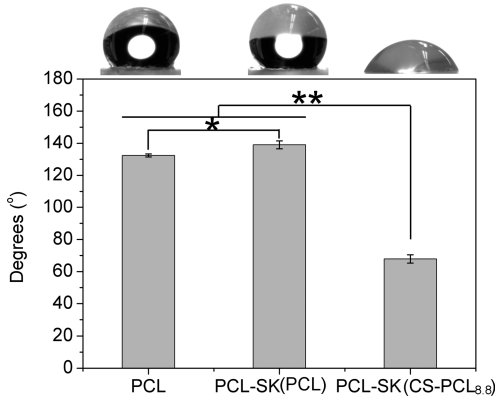

Figure 7. Water contact angles of the nanofibrous scaffolds.

introduction of CS on the surface might also be helpful for cell growth due to the good biocompatibility of chitosan.[42]

3.6. Biomimic Mineralization Behavior. When bioactive materials are implanted into the body, they will bond to bone via an apatite layer deposited on the surface.[43] Researchers have been using SBF to assess the bone-binding ability of scaffolds in vitro. Figure 8 shows the morphological evolution of mineralized PCL–SK (CS–PCL$_{8.8}$) after mineralization for 1, 3, and 7 days. After mineralization for 1 day, the nanofibers retained their shape, wrapped by the formed minerals with a periodic distance. Crystal growth occurred preferentially along the longitudinal direction of the nanofibers. After 3 days of

DOI: 10.1021/acsami.5b00900
ACS Appl. Mater. Interfaces 2015, 7, 6955–6965

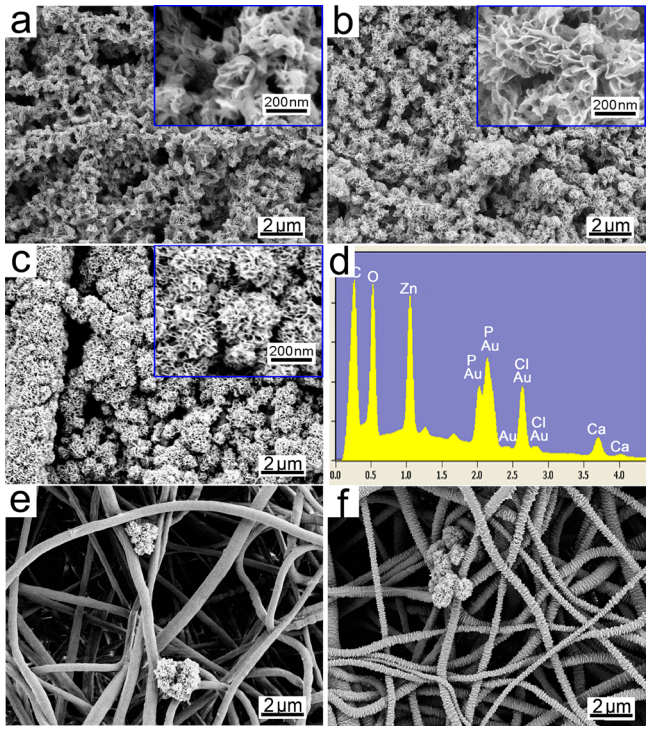

Figure 8. Morphological mineralized PCL–SK (CS–$PCL_{8.8}$) after mineralization for (a) 1, (b) 3, and (c) 7 days, (d) EDS pattern of PCL–SK (CS–$PCL_{8.8}$) after mineralization for 7 days and SEM images of (e) PCL nanofibers and (f) PCL–SK (PCL) after mineralization for 7 days.

mineralization, the fibrous and porous structure of the scaffolds was absent due to the overgrowth of apatite minerals. Seven days later, the nanofibers were completely wrapped by the deposited mineral layers, which were much thicker than at 3 days, and formed into globules. The elements of the formed minerals were detected by EDS. Both calcium and phosphorus elements were detected from the minerals, thereby indicating the formation of apatite. The control experiments were conducted on neat PCL and PCL–SK (PCL) scaffolds for up to 7 days. The morphological results of the samples after testing for 7 days are shown in Figure 8e and f, from which it was found that there were only a few deposition clusters on these scaffolds, and the minerals only presented on the surface of the scaffolds.

Previous studies have concluded that enhanced hydrophilicity and the introduction of functional groups, such as −COOH and $-NH_2$, can accelerate calcium phosphate deposition, which could lead to enrichment of Ca^{2+}, resulting in local supersaturation and crystal nucleation.[44] The in situ formation of nanohydroxyapatite on a chitosan-gelatin network has also been studied and it was found that the carboxyl groups of gelatin, carbonyl groups, and amino groups of gelatin and chitosan play a key role in the formation of hydroxyapatite.[45] In this work, the introduction of chitosan via induced crystallization of CS–PCL copolymers on the electrospun PCL nanofibers successfully induced fast and uniform calcium phosphate deposition on the scaffolds. The improved hydrophilicity and introduced anionic groups by chitosan onto the scaffolds could be the result of accelerated mineral deposition. However, the PCL and PCL–SK (PCL) scaffolds exhibited hydrophobicity and a relatively inert surface, which resulted in low apatite deposition.[46]

3.8. Biocompatibility Evaluations. *3.8.1. Cell Attachment and Cytoskeleton Investigation.* The process of cell adhesion on biomaterials is comprised of a cascade of four different partly overlapping events: cell attachment, cell spreading, organization of actin cytoskeleton, and formation of focal adhesions.[47] In the initial attachment step, cells contact the scaffold surface and some ligand occurs that allow cells to attach on the scaffold. This is the foundation for cell growth on the scaffold. Cell attachment on the scaffold after culturing 4 h was investigated by staining the cell nucleus using DAPI. The results are shown in Figure S3. It was found that the cell attachment on PCL–SK (PCL) scaffolds was higher than that of neat PCL scaffolds. The reason for this is that the enhanced surface roughness from the shish-kebab structure was helpful for cell attachment.[48] The PCL–SK (CS–$PCL_{8.8}$) scaffolds supported the highest cell attachment compared with others tested due to the biologically relevant binding sites of the chitosan domains present on the surface of the PCL–SK (CS–$PCL_{8.8}$) scaffolds.[49]

The surface properties of scaffolds play a pivotal role in regulating cell growth on the scaffolds and directly influence the

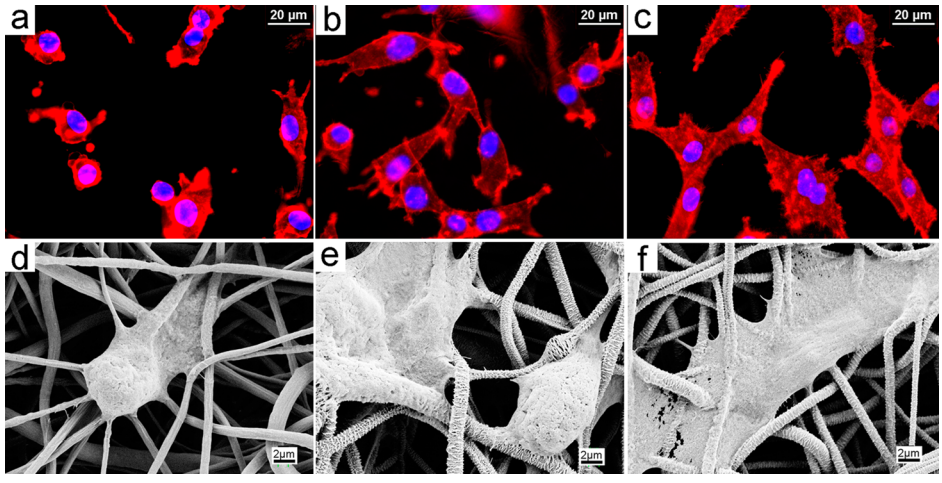

Figure 9. Cytoskeleton and SEM images of cells grown on (a, d) PCL, (b, e) PCL–SK(PCL), and (c, f) PCL–SK(CS–$PCL_{8.8}$) scaffolds after culturing 24 h.

DOI: 10.1021/acsami.5b00900
ACS Appl. Mater. Interfaces 2015, 7, 6955–6965

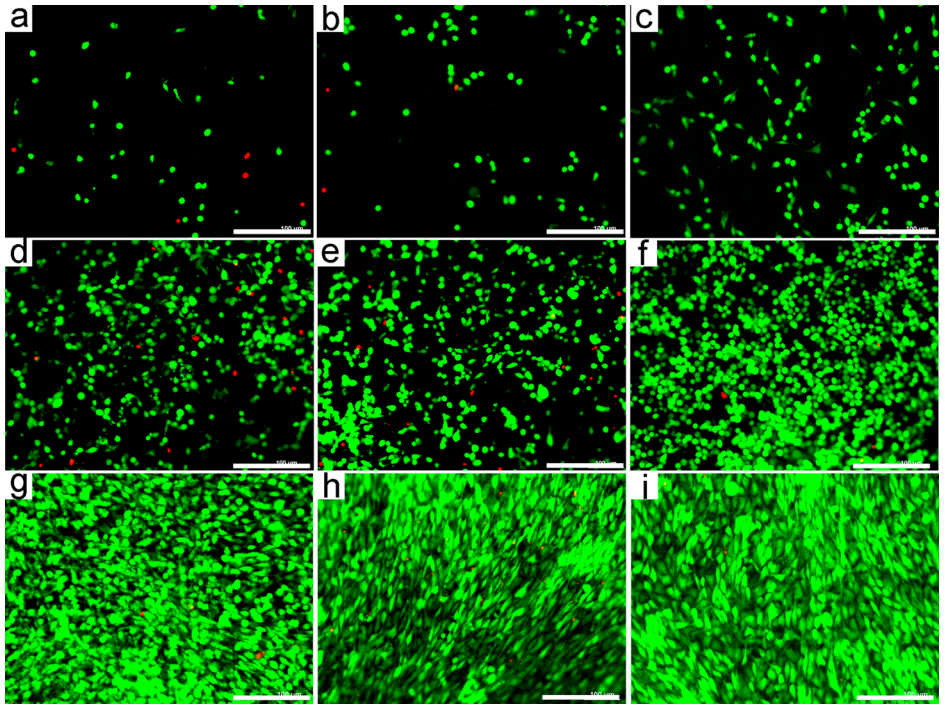

Figure 10. Day 3, 7, and 14 live/dead cell assays showing MG63 cells cultured on (a, d, g) PCL, (b, e, h) PCL−SK (PCL), and (c, f, i) PCL−SK (CS−$PCL_{8.8}$) scaffolds (the images on the first, second and third rows are the results of Day 3, 7, and 14). Live cells showed green fluorescence and red fluorescence represented dead cells (scale bar = 200 μm).

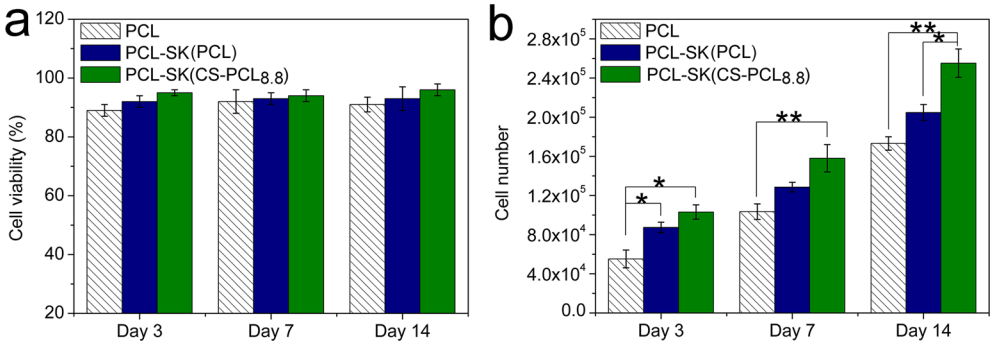

Figure 11. (a) Cell viability based on live/dead assay after culturing for 3 days, 7 days, and 14 days. (b) Proliferation of MG63 cells on the scaffolds after culturing for 3 days, 7 days, and 14 days determined by MTS assay (*p<0.05, **p<0.01).

cell response. The cytoskeleton of MG63 cells growing on scaffolds was assessed by actin staining followed by SEM observation to clearly detect the cell shape on the scaffolds. The organization of actin structures of cells on the different scaffolds were compared as shown in Figure 9. Most cells grown on the neat PCL nanofibrous scaffolds showed a spherical or narrow shape, which is a nonadherent and nonspreading morphology of cells on scaffolds (as shown in Figure 9a and d). By contrast, cells showed a higher spreading morphology on the PCL−SK (PCL) scaffolds. Moreover, it is interesting to find that cells on the PCL−SK (CS−$PCL_{8.8}$) scaffolds showed a more spreading morphology than cells on PCL−SK (PCL) scaffolds, with clearly extended pseudopodia showing up on the bodies of the cells.

3.8.2. Cell Viability and Proliferation. Cell viability assays were performed on the scaffolds and the obtained results are shown in Figures 10 and 11a. After 3 days of culture, most cells were alive (indicated by green fluorescence), with few dead cells (shown in red color in the images) detected on the three groups of scaffolds indicating nontoxicity of the scaffolds. Compared with the rounded cells on PCL scaffolds, cells on PCL−SK (PCL) are more spread. However, more flattened and stretched cells with higher viability on PCL−SK (CS−$PCL_{8.8}$) were observed, suggesting a flourishing living state of cells. After 7 and 14 days of culture, more cells were observed on all three groups of scaffolds, with the cells living better on the PCL−SK (CS−$PCL_{8.8}$) scaffolds. Furthermore, cell viability on the CS−PCL shish-kebab structured scaffolds was higher than 95%, followed by PCL−SK (PCL) and PCL (as shown in Figure 11a).

Consistent with the cell adhesion and viability results, it was found that the PCL−SK (CS−$PCL_{8.8}$) scaffolds supported the highest degree of cell proliferation, as shown in Figure 11b. After 3 days of culture, the cell population on the PCL−SK (PCL) scaffolds was higher than on the PCL scaffolds, but still lower than on the PCL−SK (CS−$PCL_{8.8}$) scaffolds, indicating that the enhanced surface roughness and the appearance of CS domains were favorable for cell growth. After 7 days of culture,

DOI: 10.1021/acsami.5b00900
ACS Appl. Mater. Interfaces 2015, 7, 6955−6965

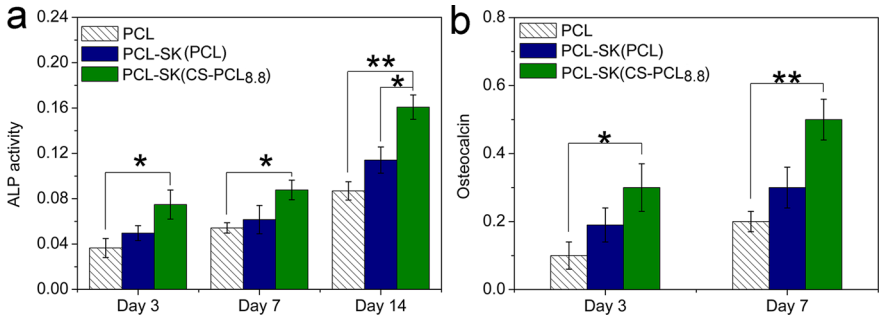

Figure 12. (a) Alkaline phosphatase (ALP) activity of cells on the scaffolds after culturing for 3 days, 7 days, and 14 days. (b) Osteocalcin expression of cells on the scaffolds after 7 days and 14 days of culture (*p<0.05, **p<0.01).

the cell population on all scaffolds was much higher than that on Day 3. The cell number on the PCL−SK (CS−$PCL_{8.8}$) scaffold was significantly higher than on the PCL−SK (PCL) or PCL scaffolds. The same result remained after 14 days of culture. Therefore, it can be concluded that the enhanced surface roughness by the shish-kebab structure facilitated cell attachment and proliferation, with the introduction of CS−PCL kebabs providing integrin binding sites, thus resulting in even greater cell viability and proliferation.

3.8.3. ALP Activity and Osteocalcin Expression of Cells on the Scaffolds. To evaluate the differentiation behavior of MG63 cells on the scaffolds, we performed alkaline phosphate activity (ALP activity) and osteocalcin expression measurements.[50] ALP, which is commonly expressed by preosteoblasts and mineralizing osteoblasts as well as MG63 cells, is often used as an early marker for osteoblast differentiation. In addition, osteocalcin is typically used as a later maker of bone biomineralization.[51] ALP activity results are shown in Figure 12a, which shows increased ALP intensity with an increase of culture time. When compared with PCL scaffolds, there was a significant increase of ALP activity of cells on PCL−SK (CS−$PCL_{8.8}$) scaffolds for all tested time points, indicating that the formation of the shish-kebab structure and the presence of chitosan molecules enhanced the osteoblast-like activity of the MG63 cells. It has been reported that greater cytoskeletal tension of cells has been linked to enhanced ALP activity,[52] which is in agreement with our results. Cells grown on PCL−SK (CS−$PCL_{8.8}$) scaffolds, which showed elongated morphologies and enhanced cytoskeletal tension (recall Figure 9), had high ALP activity and differentiation ability. Moreover, according to the osteocalcin expression results (Figure 12 (b)), the PCL−SK (CS−$PCL_{8.8}$) scaffolds showed the highest osteocalcin activity, also attributed to the shish-kebab structure formed by the CS−PCL copolymer. These results demonstrated that the PCL−SK (CS−$PCL_{8.8}$) scaffolds could stimulate MG63 cell to differentiate toward osteoblast-like cells and that these scaffolds have the potential of being used in bone tissue engineering.

4. CONCLUSIONS

In this study, scaffolds with a special structure were prepared by combining electrospinning and controlled copolymer crystallization, which not only endowed a shish-kebab structure, but also introduced the biocompatibility of natural biopolymers. Chitosan−PCL copolymers with various molar ratios were synthesized. Electrospun PCL nanofibers were used as the shish to induce crystallization of PCL domains in the CS−PCL copolymers. The CS−PCL copolymer with CS:PCL = 1:36 formed uniform kebabs on the PCL fibers, while the structure formed by CS−PCL (CS:PCL = 1:12) was irregular due to excess chitosan molecules. XPS analysis demonstrated the presence of chitosan on the surface of the prepared scaffolds. The exposed chitosan backbone on the PCL−SK (CS−$PCL_{8.8}$) scaffolds rendered a higher hydrophilicity than those comprised of PCL. These scaffolds exhibited excellent mineralization ability in SBF as well. MG63 cells were cultured on the prepared scaffolds for up to 14 days to verify cell attachment, viability, proliferation, and differentiation abilities. The results demonstrated that the PCL−SK (CS−$PCL_{8.8}$) scaffolds were the most favorable for cell growth, with enhanced cell attachment, higher cell viability, and good interaction with scaffolds, as well as a better ability to form bones. Therefore, the prepared PCL fibrous scaffolds that possessed CS−PCL kebabs could be promising candidates to be used in bone tissue engineering in the future.

■ ASSOCIATED CONTENT

Supporting Information

Polarized optical microscopy (POM), tensile testing, in vitro cell culture and seeding, cell attachment, cytoskeleton study, cell viability and proliferation, cell fixation for SEM, and alkaline phosphatase (ALP) activity and osteocalcin expression. This material is available free of charge via the Internet at http://pubs.acs.org.

■ AUTHOR INFORMATION

Corresponding Authors

*E-mail: pmxfpeng@scut.edu.cn.
*E-mail: turng@engr.wisc.edu.

Notes

The authors declare no competing financial interest.

■ ACKNOWLEDGMENTS

The authors would like to acknowledge the support of the Wisconsin Institute for Discovery (WID), the China Scholarship Council, the financial support of the National Nature Science Foundation of China (No. 51073061, No. 21174044), the Guangdong Nature Science Foundation (No. S2013020013855, No. 9151064101000066), and the National Basic Research Development Program 973 (No. 2012CB025902) of China.

■ REFERENCES

(1) Hutmacher, D. W. Scaffolds in tissue engineering bone and cartilage. *Biomaterials* **2000**, *21*, 2529−2543.

DOI: 10.1021/acsami.5b00900
ACS Appl. Mater. Interfaces 2015, 7, 6955−6965

(2) Hollister, S. J. Porous scaffold design for tissue engineering. *Nat. Mater.* **2005**, *4*, 518−524.
(3) Bhardwaj, N.; Kundu, S. C. Electrospinning: A fascinating fiber fabrication technique. *Biotechnol. Adv.* **2010**, *28*, 325−347.
(4) Sill, T. J.; Recum, H. A. Electrospinning: Applications in drug delivery and tissue engineering. *Biomaterials* **2008**, *29*, 1989−2006.
(5) Li, D.; Xia, Y. N. Electrospinning of nanofibers: Reinventing the wheel? *Adv. Mater.* **2004**, *16*, 1151−1170.
(6) Greiner, A.; Wendorff, J. H. Electrospinning: A fascinating method for the preparation of ultrathin fibres. *Angew. Chem., Int. Ed.* **2007**, *46*, 5670−5703.
(7) Li, W. J.; Laurencin, C. T.; Caterson, E. J.; Tuan, R. S.; Ko, F. K. Electrospun nanofibrous structure: A novel scaffold for tissue engineering. *J. Biomed. Mater. Res.* **2002**, *60*, 613−621.
(8) Cui, W. G.; Zhou, Y.; Chang, J. Electrospun nanofibrous materials for tissue engineering and drug delivery. *Sci. Technol. Adv. Mater.* **2010**, *11*, No. 014108, DOI: 10.1088/1468-6996/11/1/014108.
(9) Venugopal, J.; Ma, L. L.; Yong, T.; Ramakrishna, S. In vitro study of smooth muscle cells on polycaprolactone and collagen nanofibrous matrices. *Cell Biol. Int.* **2005**, *29*, 861−867.
(10) Cai, K. Y.; Yao, K. D.; Cui, Y. L.; Yang, Z. M.; Li, X. Q.; Xie, H. Q.; Qing, T. W.; Gao, L. B. Influence of different surface modification treatments on poly(D,L-lactic acid) with silk fibroin and their effects on the culture of osteoblast in vitro. *Biomaterials* **2002**, *23*, 1603−1611.
(11) Feng, B.; Tu, H. B.; Yuan, H. H.; Peng, H. J.; Zhang, Y. Z. Acetic-acid-mediated miscibility toward electrospinning homogeneous composite nanofibers of GT/PCL. *Biomacromolecules* **2012**, *13*, 3917−3925.
(12) Jing, X.; Salick, M. R.; Cordie, T.; Mi, H. Y.; Peng, X. F.; Turng, L. S. Electrospinning homogeneous nanofibrous poly(propylene carbonate)/gelatin composite scaffolds for tissue engineering. *Ind. Eng. Chem. Res.* **2014**, *53*, 9391−9400.
(13) Jing, X.; Mi, H. Y.; Cordie, T. M.; Salick, M. R.; Peng, X. F.; Turng, L. S. Fabrication of shish-kebab structured poly(ε-caprolactone) electrospun nanofibers that mimic collagen fibrils: Effect of solvents and matrigel functionalization. *Polymer* **2014**, *55*, 5396−5406.
(14) Cui, W. G.; Cheng, L. Y.; Li, H. Y.; Zhou, Y.; Zhang, Y. G.; Chang, J. Preparation of hydrophilic poly(L-lactide) electrospun fibrous scaffolds modified with chitosan for enhanced cell biocompatibility. *Polymer* **2012**, *53*, 2298−2305.
(15) Cheng, Z. Y.; Teoh, S. H. Surface modification of ultra thin poly (epsilon-caprolactone) films using acrylic acid and collagen. *Biomaterials* **2004**, *25*, 1991−2001.
(16) Webster, T. J.; Ergun, C.; Doremus, R. H.; Siegel, R. W.; Bizios, R. Specific proteins mediate enhanced osteoblast adhesion on nanophase ceramics. *J. Biomed. Mater. Res.* **2000**, *51*, 475−483.
(17) Woo, K. M.; Chen, V. J.; Ma, P. X. Nano-fibrous scaffolding architecture selectively enhances protein adsorption contributing to cell attachment. *J. Biomed. Mater. Res., Part A* **2003**, *67A*, 531−537.
(18) Bai, H. W.; Huang, C. M.; Xiu, H.; Zhang, Q.; Deng, H.; Wang, K.; Chen, F.; Fu, Q. Significantly improving oxygen barrier properties of polylactide via constructing parallel-aligned shish-kebab-like crystals with well-interlocked boundaries. *Biomacromolecules* **2014**, *15*, 1507−1514.
(19) Fujita, M.; Takikawa, Y.; Teramachi, S.; Aoyagi, Y.; Hiraishi, T.; Doi, Y. Morphology and enzymatic degradation of oriented thin film of ultrahigh molecular weight poly[(*R*)-3-hydroxybutyrate]. *Biomacromolecules* **2004**, *5*, 1787−1791.
(20) Wang, X. F.; Salick, M. R.; Wang, X. D.; Cordie, T.; Han, W. J.; Peng, Y. Y.; Li, Q.; Turng, L. S. Poly(epsilon-caprolactone) nanofibers with a self-induced nanohybrid shish-kebab structure mimicking collagen fibrils. *Biomacromolecules* **2013**, *14*, 3557−3569.
(21) Rajzer, I.; Menaszek, E.; Kwiatkowski, R.; Planell, J. A.; Castano, O. Electrospun gelatin/poly(epsilon-caprolactone) fibrous scaffold modified with calcium phosphate for bone tissue engineering. *Mater. Sci. Eng., C* **2014**, *44*, 183−190.
(22) Lee, P.; Tran, K.; Chang, W.; Shelke, N. B.; Kumbar, S. G.; Yu, X. J. Influence of chondroitin sulfate and hyaluronic acid presence in nanofibers and its alignment on the bone marrow stromal cells: Cartilage regeneration. *J. Biomed. Nanotechnol.* **2014**, *10*, 1469−1479.
(23) Rajzer, I. Fabrication of bioactive polycaprolactone/hydroxyapatite scaffolds with final bilayer nano-/micro-fibrous structures for tissue engineering application. *J. Mater. Sci.* **2014**, *49*, 5799−5807.
(24) Williams, J. M.; Adewunmi, A.; Schek, R. M.; Flanagan, C. L.; Krebsbach, P. H.; Feinberg, S. E.; Hollister, S. J.; Das, S. Bone tissue engineering using polycaprolactone scaffolds fabricated via selective laser sintering. *Biomaterials* **2005**, *26*, 4817−4827.
(25) Zhang, X. J.; Chang, W.; Lee, P.; Wang, Y. H.; Yang, M.; Li, J.; Kumbar, S. G.; Yu, X. J. Polymer-ceramic spiral structured scaffolds for bone tissue engineering: Effect of hydroxyapatite composition on human fetal osteoblasts. *PLoS One* **2014**, DOI: 10.1371/journal.-pone.0085871.
(26) Yang, X. C.; Chen, X. N.; Wang, H. J. Acceleration of osteogenic differentiation of preosteoblastic cells by chitosan containing nanofibrous scaffolds. *Biomacromolecules* **2009**, *10*, 2772−2778.
(27) Sasmazel, H. T. Novel hybrid scaffolds for the cultivation of osteoblast cells. *Int. J. Biol. Macromol.* **2011**, *49*, 838−846.
(28) Skotak, M.; Leonov, A. P.; Larsen, G.; Noriega, S.; Subramanian, A. Biocompatible and biodegradable ultrafine fibrillar scaffold materials for tissue engineering by facile grafting of L-lactide onto chitosan. *Biomacromolecules* **2008**, *9*, 1902−1908.
(29) Chen, H. L.; Fan, X. Q.; Xia, J.; Chen, P.; Zhou, X. J.; Huang, J.; Yu, J. H.; Gu, P. Electrospun chitosan-graft-poly(epsilon-caprolactone)/poly(epsilon-caprolactone) nanofibrous scaffolds for retinal tissue engineering. *Int. J. Nanomed.* **2011**, *6*, 453−461.
(30) Kokubo, T.; Takadama, H. How useful is SBF in predicting in vivo bone bioactivity? *Biomaterials* **2006**, *27*, 2907−2915.
(31) Weinhold, M. X.; Sauvageau, J. C. M.; Keddig, N.; Matzke, M.; Tartsch, B.; Grunwald, I.; Kubel, C.; Jastorff, B.; Thoming, J. Strategy to improve the characterization of chitosan for sustainable biomedical applications: SAR guided multi-dimensional analysis. *Green Chem.* **2009**, *11*, 498−509.
(32) Zhou, S. B.; Deng, X. M.; Yang, H. Biodegradable poly(epsilon-caprolactone)-poly(ethylene glycol) block copolymers: Characterization and their use as drug carriers for a controlled delivery system. *Biomaterials* **2003**, *24*, 3563−3570.
(33) Sarasam, A.; Madihally, S. V. Characterization of chitosan-polycaprolactone blends for tissue engineering applications. *Biomaterials* **2005**, *26*, 5500−5508.
(34) Dhandayuthapani, B.; Krishnan, U. M.; Sethuraman, S. Fabrication and characterization of chitosan−gelatin blend nanofibers for skin tissue engineering. *J. Biomed. Mater. Res., Part B* **2010**, *94B*, 264−272.
(35) Elzein, T.; Nasser-Eddine, M.; Delaite, C.; Bistac, S.; Dumas, P. FTIR study of polycaprolactone chain organization at interfaces. *J. Colloid Interface Sci.* **2004**, *273*, 381−387.
(36) Sarasam, A. R.; Krishnaswamy, R. K.; Madihally, S. V. Blending chitosan with polycaprolactone: Effects on physicochemical and antibacterial properties. *Biomacromolecules* **2006**, *7*, 1131−1138.
(37) Senda, T.; He, Y.; Inoue, Y. Biodegradable blends of poly(epsilon-caprolactone) with alpha-chitin and chitosan: Specific interactions, thermal properties and crystallization behavior. *Polym. Int.* **2002**, *51*, 33−39.
(38) Zhang, L. L.; Deng, X. M.; Huang, Z. T. Miscibility, thermal behaviour and morphological structure of poly(3-hydroxybutyrate) and ethyl cellulose binary blends. *Polymer* **1997**, *38*, 5379−5387.
(39) Wang, B. B.; Li, B.; Xiong, J.; Li, C. Y. Hierarchically ordered polymer nanofibers via electrospinning and controlled polymer crystallization. *Macromolecules* **2008**, *41*, 9516−9521.
(40) Yildirim, E. D.; Besunder, R.; Pappas, D.; Allen, F.; Guceri, S.; Sun, W. Accelerated differentiation of osteoblast cells on polycaprolactone scaffolds driven by a combined effect of protein coating and plasma modification. *Biofabrication* **2010**, *2*, No. 014109.
(41) Tamada, Y.; Ikada, Y. Effect of preadsorbed proteins on cell adhesion to polymer surfaces. *J. Colloid Interface Sci.* **1993**, *155*, 334−339.

DOI: 10.1021/acsami.5b00900
ACS Appl. Mater. Interfaces 2015, 7, 6955−6965

(42) Jin, H. H.; Kim, D. H.; Kim, T. W.; Shin, K. K.; Jung, J. S.; Park, H. C.; Yoon, S. Y. In vivo evaluation of porous hydroxyapatite/chitosan-alginate composite scaffolds for bone tissue engineering. *Int. J. Biol. Macromol.* **2012**, *51*, 1079−1085.
(43) Hench, L. L. Bioactive materials: The potential for tissue regeneration. *J. Biomed. Mater. Res.* **1998**, *41*, 511−518.
(44) Li, X. R.; Xie, J. W.; Yuan, X. Y.; Xia, Y. N. Coating electrospun poly(epsilon-caprolactone) fibers with gelatin and calcium phosphate and their use as biomimetic scaffolds for bone tissue engineering. *Langmuir* **2008**, *24*, 14145−14150.
(45) Li, J. J.; Chen, Y. P.; Yin, Y. J.; Yao, F. L.; Yao, K. D. Modulation of nano-hydroxyapatite size via formation on chitosan−gelatin network film in situ. *Biomaterials* **2007**, *28*, 781−790.
(46) Yang, F.; Wolke, J. G. C.; Jansen, J. A. Biomimetic calcium phosphate coating on electrospun poly(epsilon-caprolactone) scaffolds for bone tissue engineering. *Chem. Eng. J.* **2008**, *137*, 154−161.
(47) Lebaron, R. G.; Athanasiou, K. A. Extracellular matrix cell adhesion peptides: Functional applications in orthopedic materials. *Tissue Eng.* **2000**, *6*, 85−103.
(48) Deligianni, D. D.; Katsala, N. D.; Koutsoukos, P. G.; Missirlis, Y. F. Effect of surface roughness of hydroxyapatite on human bone marrow cell adhesion, proliferation, differentiation and detachment strength. *Biomaterials* **2001**, *22*, 87−96.
(49) Cooper, A.; Bhattarai, N.; Zhang, M. Q. Fabrication and cellular compatibility of aligned chitosan-PCL fibers for nerve tissue regeneration. *Carbohydr. Polym.* **2011**, *85*, 149−156.
(50) Li, M. M.; Liu, W. W.; Sun, J. S.; Xianyu, Y. L.; Wang, J. D.; Zhang, W.; Zheng, W. F.; Huang, D. Y.; Di, S. Y.; Long, Y. Z.; Jiang, X. Y. Culturing primary human osteoblasts on electrospun poly(lactic-co-glycolic acid) and poly(lactic-co-glycolic acid)/nanohydroxyapatite scaffolds for bone tissue engineering. *ACS Appl. Mater. Interfaces* **2013**, *5*, 5921−5926.
(51) Peng, F.; Yu, X. H.; Wei, M. In vitro cell performance on hydroxyapatite particles/poly(L-lactic acid) nanofibrous scaffolds with an excellent particle along nanofiber orientation. *Acta Biomater.* **2011**, *7*, 2585−2592.
(52) McBeath, R.; Pirone, D. M.; Nelson, C. M.; Bhadriraju, K.; Chen, C. S. Cell shape, cytoskeletal tension, and RhoA regulate stem cell lineage commitment. *Dev. Cell* **2004**, *6*, 483−495.

DOI: 10.1021/acsami.5b00900
ACS Appl. Mater. Interfaces 2015, 7, 6955−6965